JACS
JOURNAL OF THE AMERICAN CHEMICAL SOCIETY
Article
pubs.acs.org/JACS

Interfacial Electron Transfer into Functionalized Crystalline Polyoxotitanate Nanoclusters

Robert C. Snoeberger, III,[†] Karin J. Young,[†] Jiji Tang,[‡] Laura J. Allen,[†] Robert H. Crabtree,*[,†] Gary W. Brudvig,*[,†] Philip Coppens,*[,‡] Victor, S. Batista,*[,†] and Jason B. Benedict*[,‡]

[†]Department of Chemistry, Yale University, New Haven, Connecticut 06520-8107, United States
[‡]Department of Chemistry, University at Buffalo, State University of New York, Buffalo, New York 14260-3000, United States

Supporting Information

ABSTRACT: Interfacial electron transfer (IET) between a chromophore and a semiconductor nanoparticle is one of the key processes in a dye-sensitized solar cell. Theoretical simulations of the electron transfer in polyoxotitanate nanoclusters $Ti_{17}O_{24}(OPr^i)_{20}$ (**Ti_{17}**) functionalized with four *p*-nitrophenyl acetylacetone (**NPA-H**) adsorbates, of which the atomic structure has been fully established by X-ray diffraction measurements, are presented. Complementary experimental information showing IET has been obtained by EPR spectroscopy. Evolution of the time-dependent photoexcited electron during the initial 5 fs after instantaneous excitation to the **NPA** LUMO + 1 has been evaluated. Evidence for delocalization of the excitation over multiple chromophores after excitation to the **NPA** LUMO + 2 state on a 15 fs time scale is also obtained. While chromophores are generally considered electronically isolated with respect to neighboring sensitizers, our calculations show that this is not necessarily the case. The present work is the most comprehensive study to date of a sensitized semiconductor nanoparticle in which the structure of the surface and the mode of molecular adsorption are precisely defined.

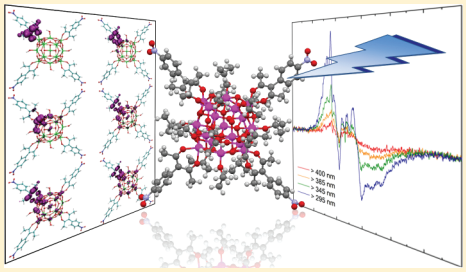

INTRODUCTION

Dye-sensitized solar cells (DSSC) promise the environmentally friendly and cost-effective conversion of solar light into fuels and/or electricity.[1−4] DSSCs are driven by photoinduced interfacial electron transfer (IET), which injects photoexcited electrons from the dye sensitizer into the conduction band of the semiconductor substrate. Naturally, the interfaces are critical to performance and much attention has been directed to them via experiment, theory, and computational modeling.[5−8] However, due to the complexity of the surfaces, including the presence of multiple exposed facets and binding sites as well as surface defects and impurities, the correlation between experiment and simulations based on pristine surfaces remains uncertain. Here, we bridge the gap between theoretical modeling, crystallography, and spectroscopy by studying IET in functionalized polyoxotitanate (POT) nanocrystals $Ti_{17}O_{24}(OPr^i)_{20}$ (**Ti_{17}**) of which the structure has been precisely determined by X-ray diffraction. The precise structural information enables time-dependent electronic structure calculations that predict photoinduced IET in this model system. The sensitization of the nanoparticle by the acetylacetonate-anchored chromophore is confirmed spectroscopically by an increase in the onset of the photoinduced titanium and oxygen EPR signals from approximately 300 nm and lower for the unfunctionalized cluster to over 400 nm in the case of the functionalized nanoparticle. The comprehensive analysis described should contribute to a more detailed understanding of the chemistry and photophysics of sensitized semiconductor interfaces.

The structure of the interface can greatly influence the rate and efficiency of IET.[5,9] In the case of the dye/semiconductor interface, strong electronic coupling between the dye excited state and the conduction band is desirable for ultrafast electron transfer. Fast injection into the semiconductor minimizes losses due to radiative and nonradiative relaxation of the dye excited state. We have recently shown that a new class of derivatized acetylacetonate (acac) linkers can functionalize pure phase TiO_2 nanoparticles and be used to anchor photocatalytically active manganese complexes to the surface.[10,11] These acac linkers provide robust coupling to the semiconductor substrate under aqueous and oxidative conditions. The characterization of the acac anchor binding mode to the TiO_2 surface has been only indirect, based on computational modeling and UV/vis and IR spectroscopy as in previous studies.[8,10−16] Here, we structurally resolve TiO_2 surfaces functionalized by acac linkers by using X-ray diffraction methods.

POT clusters functionalized with catechol and isonicotinic acid have been proposed as models for the sensitizer/semiconductor interfaces in DSSCs.[17] POT clusters are attractive analogues for pure phase TiO_2 nanoparticles since they possess structural features of bulk crystals, including similar coordination and connectivity, as well as features associated with nanoparticles, such as reactive four- and five-coordinate Ti^{4+} centers[18] and size-dependent band gaps.[19] The clusters are also attractive building blocks due to their

Received: February 7, 2012
Published: May 1, 2012

   dx.doi.org/10.1021/ja301238t | J. Am. Chem. Soc. 2012, 134, 8911−8917

propensity to assemble into single crystals suitable for X-ray structure determination at atomic resolution.[20,21] Here, we focus on the functionalization of the POT cluster $Ti_{17}O_{24}(OPr^i)_{20}$ (**Ti_{17}**) with the model sensitizer *p*-nitrophenyl acetylacetone (**NPA-H**) and the subsequent crystallization of the product to gain atomic resolution structural information about the sensitizer/semiconductor interface in these particles. The light-induced charge-separated states in functionalized and unfunctionalized POT clusters are compared by EPR spectroscopy and analyzed by quantum dynamics simulations of IET, providing a detailed description of charge injection for a structurally resolved sensitizer/semiconductor interface.

EXPERIMENTAL AND COMPUTATIONAL PROCEDURES

Chemicals. All reagents and solvents were purchased from commercial sources. Benzene (anhydrous, 99.9%, Alfa Aesar) was degassed prior to transfer and storage in a glovebox. All compounds containing titanium were stored and handled in a glovebox under an argon atmosphere. **Ti_{17}** was prepared according to previously reported methods.[22]

3-(4-Nitrophenyl)pentane-2,4-dione (NPA-H). The synthesis of **NPA-H** was carried out in an analogous manner to the preparation used by Jiang et al.[23] to synthesize 3-(3-nitrophenyl)pentane-2,4-dione. A mixture of 1-iodo-4-nitrobenzene (2.0 mmol), 2,4-pentanedione (6.0 mmol), cesium carbonate (8.0 mmol), freshly recrystallized copper(I) iodide (0.20 mmol), and L-proline (0.40 mmol) in dry DMSO (10 mL) was wrapped in aluminum foil to protect from it light and heated at 70 °C under nitrogen atmosphere for 24 h. The cooled solution was poured into 1 M HCl and extracted with ethyl acetate. The organic layer was washed with water and brine and dried over Na_2SO_4, and the solvent was removed in vacuo. The crude residue was purified by silica gel flash column chromatography, using a mixture of hexanes:ethyl acetate (7:3) as eluent to afford 292 mg (66% yield) of **NPA-H** as a yellow solid. The product was then recrystallized from hexanes to give a slightly yellow crystalline solid. ^{1}H NMR (400 MHz, $CDCl_3$): δ 16.78 (s, 1H), 8.27 (dd, J = 2.1, 8.9, 2H), 7.39 (dd, J = 2.1, 8.9, 2H), 1.90 (s, 6H). ^{13}C NMR ($CDCl_3$, 500 MHz): δ 190.5, 147.3, 144.0, 132.1, 124.0, 113.6, 24.2. HRMS: calcd (found) for $C_{11}H_{11}NO_4$ M^+ 222.076084, found 222.07611.

$Ti_{17}O_{24}(OPr^i)_{16}(NPA)_4$ ($Ti_{17}NPA_4$). To a 20 mL vial containing **Ti_{17}** (26.9 mg, 11.3 μmol) dissolved in 5.0 mL of benzene was added a solution of **NPA-H** (10.0 mg, 45.2 μmol) dissolved in 5.0 mL of benzene. The vial was loosely capped and allowed to slowly evaporate over a period of 2–3 days. After this time, pale yellow (nearly colorless) crystals suitable for single crystal X-ray diffraction were obtained.

Crystals obtained from a benzene solution are only stable in oil for 20–40 s. After numerous attempts, a single crystal 0.4 × 0.2 × 0.2 mm^3 was rapidly mounted on a glass fiber in oil and cooled to 90 K. The rapid decomposition of the crystals is likely due to the presence of seven benzene molecules per **$Ti_{17}NPA_4$** in the lattice.

Data Collection. X-ray diffraction data were collected on a Bruker SMART APEX2 CCD diffractometer installed with a Rigaku RU-200 rotating anode source (Mo Kα, λ = 0.710 73 Å) and equipped with an Oxford Cryosystems nitrogen gas flow apparatus. Data were collected at 90 K with a crystal to detector distance of 40 mm. Five ω-scans (180°/scan, 0.5°/frame) were collected with an exposure time of 30 s per frame.

EPR Spectroscopy. Samples for EPR spectroscopy were prepared in a glovebox under N_2 atmosphere by dissolving 5 mg of **Ti_{17}** or **$Ti_{17}NPA_4$** in 2 mL of 2:1 dichloromethane:benzene and transferring approximately 200 μL of this sample to a 4 mm OD quartz EPR tube. Samples were frozen in liquid N_2 before being transferred to the cryostat. EPR spectra were measured at 7 K in perpendicular mode on a Bruker ELEXYS E500 spectrometer equipped with an SHQ cavity and Oxford ESR 900 liquid helium cryostat. Samples were illuminated in the cryostat at 7 K using a 1000 W Xe arc lamp equipped with a water filter and various long-pass filters. Spectra were recorded with the following settings: microwave frequency = 9.391 GHz, microwave power = 1.0 mW, modulation amplitude = 4 G, modulation frequency = 100 kHz.

Computational Model. The crystal structure of $[Ti_{17}O_{24}(OPr^i)_{16}(NPA)_4]$ was used as the initial structure and optimized to the minimum energy configuration as determined by density functional theory (DFT), using the B3LYP exchange–correlation functional, with the LACVP basis set by using the computational chemistry package Jaguar 7.[24] The models were simplified by replacing OPr^i groups by OH groups, giving the model structure $[Ti_{17}O_{24}(OH)_{16}(NPA)_4]$. The rmsd of the Ti atoms between the crystal structure and the relaxed DFT model structure is 0.05 Å, indicating the similarity of the models and confirming that replacing OPr^i by OH induces only minor structural rearrangements.

It is well-known that time-dependent density functional theory (TDDFT) yields substantial errors for the excitation energies of charge-transfer (CT) excited states, when approximate standard exchange–correlation (xc) functionals are used, such as SVWN, BLYP, or B3LYP.[25−27] Also, the correct $1/R$ asymptotic behavior of CT states with respect to a distance coordinate R between the separated charges of the CT state is not reproduced by TDDFT employing these xc-functionals.[25,28,29] The first failure is due to the self-interaction error in the orbital energies from the ground-state DFT calculation, while the latter is a similar self-interaction error in TDDFT arising through the electron transfer in the CT state.[30]

Electron Transfer Dynamics. To characterize the IET time scale, the survival probability, $P_{MOL}(t)$, defined as the probability that the photoexcited electron remains in the adsorbate molecule, **NPA**, at time t after excitation of the system was computed. $P_{MOL}(t)$ was obtained as the projection of the time-evolved electronic wave function onto the atomic orbitals (AOs) of the molecular adsorbate. The survival probability was computed as $P_{MOL}(t) = |\sum_i^{MOL}\sum_j B_i^*(t)B_j(t)\mathbf{S}^{ij}|$, where **S** is the overlap matrix and B_i is a time-dependent expansion coefficient. Computing the time-dependent wave function $\Psi(t) = \sum_i B_i(t)\chi_i$, expanded in the basis set of AOs χ_i, required the propagation of the expansion coefficients $B_i(t) = \sum_q Q_i^q C_q \exp[-(i/\hbar)E_q t]$, where C_q are the expansion coefficients of the initial state. The eigenvectors and eigenvalues Q_q and E_q were obtained from the ground state electronic density using the electronic structure package Gaussian 09, Revision A.02,[31] with the electronic structure described by DFT at the B3LYP/LANL2DZ level of theory. Initial states, C_q, were defined in terms of the unoccupied orbitals of an isolated **NPA-H** molecule. Electron transfer dynamics simulations were performed on the previously relaxed **$Ti_{17}NPA_4$** system. It should be noted that theoretical models do not include losses due to radiative and nonradiative relaxation of the dye excited-state, which typically occur on the nanosecond time scale. Likewise, the simulations have been performed in the low temperature (0 K) limit where nuclear motion is much slower than electronic relaxation; thus, coupling between the electronic wave function and the molecular vibrations has not been included.

Electronic Optical Transitions. To characterize the photoexcited electrons generated by optical transitions, excited states were computed by using time-dependent density functional theory (TDDFT) at the B3LYP/LANL2DZ level, as implemented in Gaussian 09. Optical transitions were computed for both the isolated **NPA-H** molecule and the **$Ti_{17}NPA_4$** model. The minimum energy configuration of the isolated **NPA-H** molecule was obtained at the B3LYP/6-31G* level of theory.

RESULTS

The reaction between **Ti_{17}** and **NPA-H** follows the same general scheme as reported for catechol and isonicotinic acid.[17] Four equivalents of **NPA-H**, one for each reactive five-coordinate atom in **Ti_{17}**, are treated with 1 equiv of the POT cluster to give a **Ti_{17}** cluster which contains four **NPA** ligands, **$Ti_{17}NPA_4$**.

Binding Mode. An examination of the crystal structure of $\mathbf{Ti_{17}NPA_4}$ reveals that all four of the isopropoxide groups bound to the five-coordinate titaniums of the initial $\mathbf{Ti_{17}}$ cluster have each been replaced by **NPA** ligands. The **NPA** exhibits bidentate attachment to the titanium atom, increasing its coordination number from five to six. The nearly equivalent lengths of the four Ti−O bonds between the cluster and the two crystallographically independent **NPA** ligands (2.030, 2.020, 2.050, and 2.015 Å) and the lack of any residual electron density near the anchor oxygen atoms indicate that the acetylacetone (acac-H) anchor group has been deprotonated to the acetylacetonate anion (acac). Additionally, deprotonation of the **NPA-H** ligand to **NPA** conserves the charge neutrality of the cluster. It is reasonable to assume that the proton from the ligand is transferred to the displaced isopropoxide (OPr^i) group to give 2-propanol ($HOPr^i$), thus the reaction becomes

$$Ti_{17}O_{24}(OPr^i)_{20} + 4\mathbf{NPA\text{-}H} \rightarrow Ti_{17}O_{24}(OPr^i)_{16}(NPA)_4 + 4HOPr^i$$

Two modes of bidentate attachment of the acac linker to the (101) surface of anatase were investigated previously.[10] Bidentate attachment of the acetylacetonate anchor group at an oxygen vacancy on the surface of anatase was predicted to be the most energetically stable mode of attachment. The second bidentate mode resulted in the displacement of the titanium from the surface and the breaking of a subsurface Ti−O bond, a rearrangement that was energetically disfavored. Given the energetic analysis and the displacement of OPr^i by the **NPA** ligand during functionalization, it is natural to expect that the **NPA** binding motif in $\mathbf{Ti_{17}NPA_4}$ closely resembles the bidentate mode in the oxygen vacancy model of anatase.

Figure 1 shows the geometry of a fragment of $\mathbf{Ti_{17}NPA_4}$ and the two models of bidentate attachment to the anatase (101). In the case of the four Ti−O bonds that attach the Ti/O/acac fragments to the larger nanoclusters, the bond lengths of the experimental geometry (from 1.897 to 1.933 Å) are closer to the values for the oxygen vacancy model (from 1.951 to 1.980 Å) than the surface chelation model (from 2.100 to 2.157 Å). In fact, the Ti−O bond lengths of both the experimental geometry and the oxygen vacancy model are quite similar to that of bulk anatase (1.934 and 1.980 Å). The distance between the two oxygens of the acac anchor are 2.594 and 2.544 Å for the experimental geometry and the surface chelation model, respectively. The larger value of 2.787 Å observed in the oxygen vacancy model is a consequence of the fact that the oxygen atom of the anchor that fills the vacancy also interacts with a neighboring titanium atom (not shown).

While nearly 100 crystal structures containing the acac group bound to titanium have been deposited in the CSD,[32] the vast majority contain only one or two titanium atoms. Prior to this report, the largest polyoxotitanate possessing a dione ligand had only five titanium atoms in its core (WIYCOW). In every one of these Ti-acac crystal structures, bidentate chelation of the acac group to a single titanium atom was observed. In several additional crystal structures of larger Ti/O clusters containing acac groups (to be reported), the observed binding is invariably bidentate.

Charge Separation. The light-induced charge-separated state was characterized using EPR spectroscopy. Under illumination, electrons in the conduction band are localized on titanium centers, generating d^1 Ti^{3+} species, while holes are localized on oxygen atoms, producing oxygen-centered radicals.

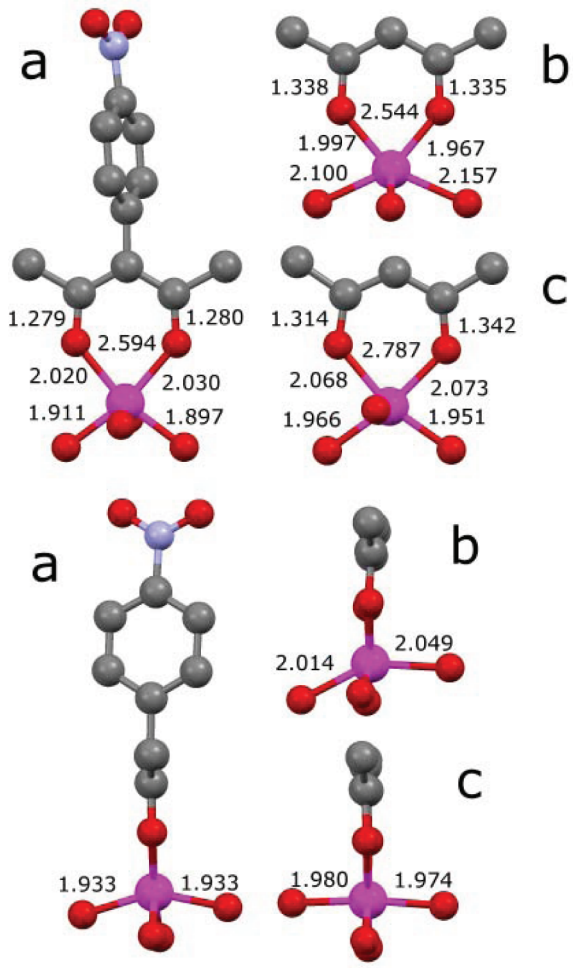

Figure 1. Two views (upper, lower) of the Ti/O/acac fragment from the crystal structure of $\mathbf{Ti_{17}NPA_4}$ (a), the surface chelation model (b), and the oxygen vacancy model (c) of acac binding to the anatase (101).[10] Titanium atoms are pink; oxygen, red; carbon, gray; nitrogen, blue. Selected bond lengths are labeled including the acac oxygen−oxygen distance.

At low temperature with continuous illumination, both paramagnetic species are long-lived and easily observed by EPR. The spectra shown for $\mathbf{Ti_{17}}$ and $\mathbf{Ti_{17}NPA_4}$ in Figure 2 indicate contributions from both titanium- and oxygen-centered unpaired electrons. The signals at $g > 2$ are assigned to oxygen anion holes, and those at $g < 2$ are assigned to titanium electrons, consistent with previous reports of charge separations in TiO_2.[33−37] Preliminary spectral simulations suggest that both regions of the spectrum are composed of three overlapping signals resulting from contributions of oxygen and titanium centers in different coordination environments. Of the three contributing titanium signals, two axial components are present in both the $\mathbf{Ti_{17}}$ and $\mathbf{Ti_{17}NPA_4}$ spectra. A third axial component changes upon coordination of the NPA ligand, suggesting that it derives from the five-coordinate titanium center in $\mathbf{Ti_{17}}$, which becomes six-coordinate upon NPA ligation. Complete analysis of the EPR results will be reported in a future publication.

The wavelength of light used to illuminate the sample may be varied with long-pass filters, used in order from longest to shortest wavelength. Comparison of the wavelength-dependent spectra of $\mathbf{Ti_{17}}$ and $\mathbf{Ti_{17}NPA_4}$ demonstrates that coordination

dx.doi.org/10.1021/ja301238t | J. Am. Chem. Soc. 2012, 134, 8911−8917

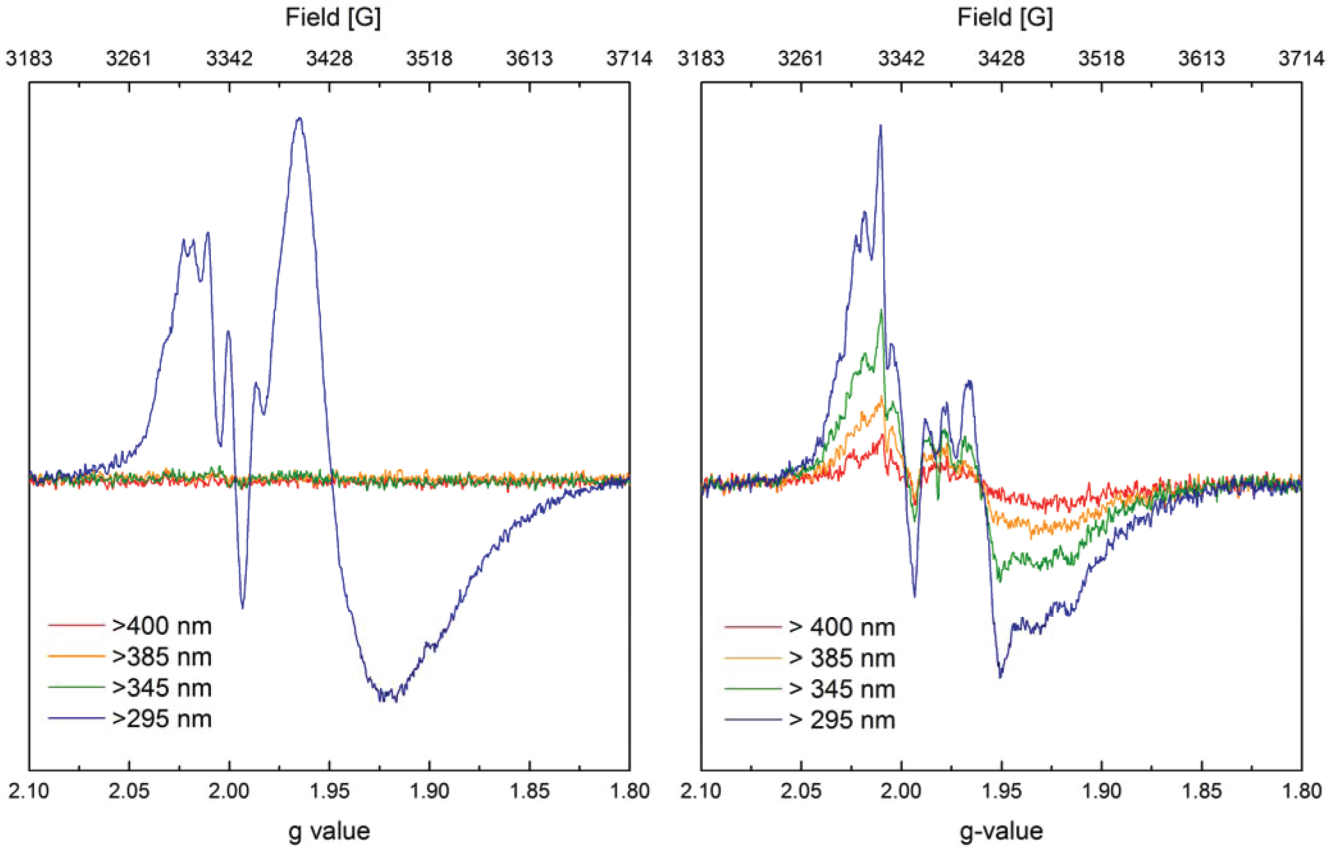

Figure 2. Light-minus-dark EPR spectra of frozen solutions of $\mathbf{Ti_{17}}$ (left) and $\mathbf{Ti_{17}NPA_4}$ (right) in 2:1 dichloromethane:benzene at 7 K. The illumination wavelengths were varied by the use of long-pass filters.

of NPA shifts the onset wavelength for charge separation. For unfunctionalized $\mathbf{Ti_{17}}$, no oxygen or titanium radicals are seen for wavelengths greater than 345 nm. However, radical formation is observed when a >295 nm filter is used, suggesting that the excitation wavelength for the onset of charge separation lies between 345 and 295 nm. By contrast, some of the charge-separated state for $\mathbf{Ti_{17}}$-$\mathbf{NPA_4}$ clusters is observed with irradiation above 400 nm, and the EPR signal intensity increases with illumination at shorter wavelengths. The transition responsible for the generation of the EPR signal is significantly shifted by the addition of the **NPA** chromophore, suggesting that $\mathbf{Ti_{17}}$ clusters are sensitized in a manner analogous to TiO_2 nanoparticles.

Interfacial Electron Transfer. Before reporting the results from the IET simulations, it is useful to look at the density of states (DOS) and projected density of states (pDOS) of the functionalized nanoparticle. The DOS for an unbound **NPA-H** molecule is included to examine the effect of ligation on the electronic structure of the sensitizer. Figure 3 shows the DOS of the $[Ti_{17}O_{24}(OH)_{16}(NPA)_4]$ model system along with the pDOS of all four **NPA** adsorbates. The DOS shows that the HOMO−LUMO gap in the model system is ∼3.5 eV, with the HOMO and LUMO (both are quasi-4-fold degenerate states) populations localized mainly on the **NPA** adsorbates, as indicated by the pDOS. The pDOS also indicates that the majority of the **NPA** orbitals are energetically unperturbed upon complexation to the $\mathbf{Ti_{17}}$ cluster with the exception of the **NPA-H** LUMO + 1. The ligand LUMO + 1 orbitals mix with the first unoccupied levels of the $\mathbf{Ti_{17}}$ cluster to form new

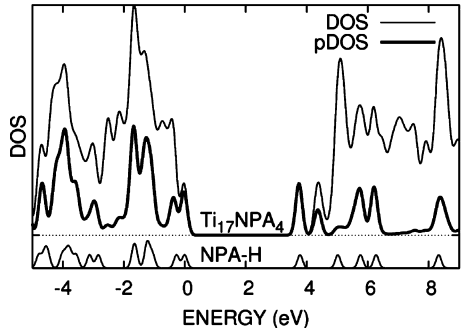

Figure 3. Density of states of $[Ti_{17}O_{24}(OH)_{16}(NPA)_4]$ with the projected density of states for all four **NPA** adsorbates. The density of states of **NPA-H** is shown for comparison with the cluster. The energies are shifted so that the $[Ti_{17}O_{24}(OH)_{16}(NPA)_4]$ HOMO is located at the origin. The density of states was convoluted with Gaussians to facilitate visualization.

ligand−metal hybrid orbitals located at ∼4.2 eV above the HOMO.

Figure 4 shows the electron density of the four initial excited states used in the IET simulations. The initial states correspond to instantaneous photoexcitations to the LUMO, LUMO + 1, LUMO + 2, and LUMO + 3 of a single **NPA** with energies of 3.72, 4.83, 5.69, and 6.19 eV, respectively. The pDOS indicates that the first excited state (i.e., the **NPA** LUMO) is located below the unoccupied Ti/O orbitals of the cluster, indicating that IET from that state is unlikely to be observed. The remaining states are aligned with a large density of unoccupied

dx.doi.org/10.1021/ja301238t | J. Am. Chem. Soc. 2012, 134, 8911−8917

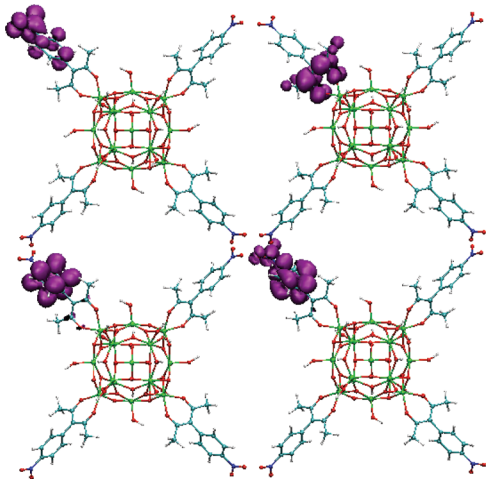

Figure 4. Image of the electron density of the initial states used in the IET simulations. The electronic densities correspond to the **NPA** LUMO (top left), LUMO + 1 (top right), LUMO + 2 (bottom left), and LUMO + 3 (bottom right). Titanium atoms are green; oxygen, red; carbon, cyan; nitrogen, blue; and hydrogen, white.

Ti_{17} cluster levels, especially the LUMO + 1, indicating that IET could occur from these states.

Figure 5 shows the survival probability $P(t)$ for an electron starting from one of the three initial states that overlap

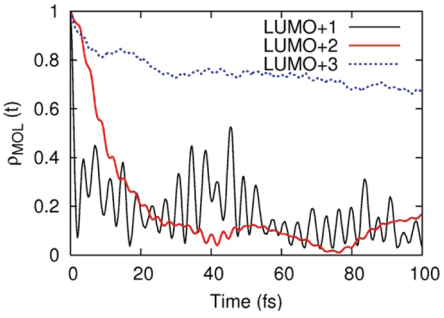

Figure 5. Survival probability for the photoexcited electron to remain on the **NPA** adsorbate after instantaneous photoexcitation to the LUMO + 1 (solid black), LUMO + 2 (solid red), or LUMO + 3 (dashed blue) of a single **NPA** that is a piece of the larger $[Ti_{17}O_{24}(OH)_{16}(NPA)_4]$ structure.

energetically with Ti/O orbitals: the LUMO + 1, LUMO + 2, and LUMO + 3 of the **NPA** adsorbate. The simulation using the **NPA** LUMO initial state resulted in a survival probability that shows minimal population transfer, <1%, of the photoexcited electron during the first 1 ps of dynamics and was not included in the figure. Thus, no injection can occur from photoexcited electrons populating the **NPA** LUMO. Charge injection from the NPA LUMO + 1 to the Ti/O cluster occurs extremely rapidly as $P(t)$ falls to nearly zero within 1−2 fs (Figures 5 and 6). Following electronic excitation, strongly coupled nondegenerate quantum mechanical systems generally exhibit Rabi oscillations, which are readily observed for IET from the LUMO + 1 and LUMO + 2 states. The larger oscillations and nonexponential behavior of the IET from the LUMO + 1 are a consequence of the finite number of empty Ti_{17} orbitals available at this energy.[38]

The simulation of IET, using the **NPA** LUMO + 2 as the initial state, shows ultrafast IET with an injection time scale of

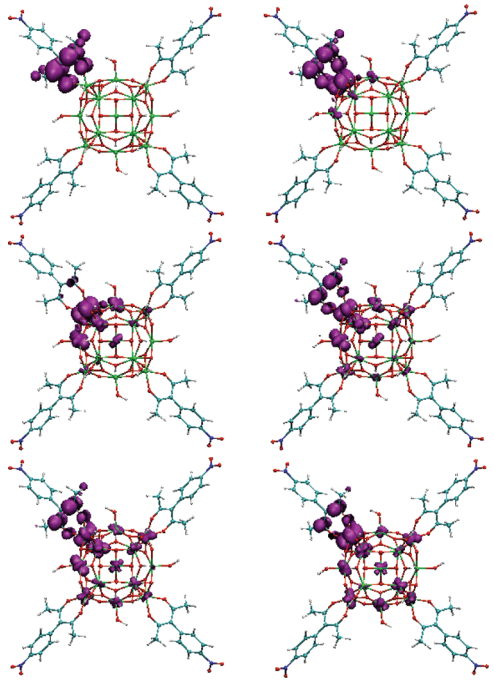

Figure 6. Evolution of the time-dependent photoexcited electron during the initial 5 fs of dynamics after instantaneous excitation to the **NPA** LUMO + 1. Each panel shows a snapshot of the electronic density at 1 fs intervals, progressing from left to right and then from top to bottom. Titanium atoms are green; oxygen, red; carbon, cyan; nitrogen, blue; and hydrogen, white.

approximately 12 fs. The **NPA** LUMO + 3 initial state shows fast initial IET, transferring about 20% of the electron population in the first 10 fs, followed by a much slower rate of IET. It is interesting that a large difference in the survival probability is obtained for the third and fourth initial states, since the density of unoccupied **Ti_{17}** cluster states is similar at the energy of the initial states.

Figure 6 shows snapshots of the time-evolved electron density after instantaneous photoexcitation of the functionalized nanocrystal to the **NPA** LUMO + 1 (the second excited state). The **NPA** LUMO + 1 state is electronically coupled to the **Ti_{17}** cluster through the d orbitals of Ti chelated by the NPA moiety. The electron flows rapidly into the cluster with the population distributed to almost every Ti ion within 5 fs. Figure S2 (Supporting Information) shows snapshots of the first 15 fs of electron dynamics after instantaneous photoexcitation to the **NPA** LUMO + 2 on a 3 fs interval. The LUMO + 2 appears to couple to the **Ti_{17}** cluster through the same Ti d orbital as seen for excitation to the **NPA** LUMO + 1. Similar to the LUMO + 1 dynamics, the electron injected from the LUMO + 2 state is distributed to all the Ti ions in the cluster. In both cases, IET leads to electron density accumulating on a second **NPA** adsorbed directly across the **Ti_{17}** cluster from the **NPA** adsorbate where the excited electron originated. Such multichromophore delocalization arises from *indirect* coupling of the adsorbate orbitals through near-resonant states in the conduction band. Because the rate of ET is proportional to the square of the electronic coupling and the electronic coupling is determined by the orbital overlap, multichromophore delocalization is only observed on longer time scales (beyond ∼15 fs).

dx.doi.org/10.1021/ja301238t | *J. Am. Chem. Soc.* 2012, 134, 8911−8917

Electronic Transitions. The simulations of IET indicate that ultrafast injection will occur from the **NPA** LUMO + 1 and LUMO + 2 but not from the **NPA** LUMO. It is important to see if an allowed optical transition will promote an electron into the LUMO + 1 or LUMO + 2 of **NPA** (Table S8, Supporting Information). The lowest energy transition of the isolated **NPA**, as computed using TDDFT, is a HOMO−LUMO transition at 349 nm with an oscillator strength of 0.0267 atomic units (au). Unfortunately, as seen from the IET simulations, the **NPA** LUMO is below the energy level of the unoccupied $\mathbf{Ti_{17}}$ states and this excited state is predicted not to undergo ultrafast IET. While the **NPA** HOMO to LUMO + 1 does contribute to the fourth excited state, which is a weak transition at 300 nm, it is the predominant component of the much stronger seventh transition occurring at 258 nm with an oscillator strength of 0.1275 au, which also has considerable HOMO−LUMO + 2 character. The ninth electronic transition is also a relatively strong transition with an oscillator strength of 0.0938 au and is primarly HOMO to LUMO + 2 with considerable HOMO−LUMO + 1 character. Even though there are no electronic transitions in the visible region for this model sensitizer, the HOMO−LUMO + 1 and LUMO + 2 transitions are optically strong and, thus, suitable candidates for charge injection. Furthermore, it is possible that a direct transition from the **NPA** to unoccupied levels of the $\mathbf{Ti_{17}}$ cluster is allowed with a corresponding excitation wavelength in the visible region, according to the usual type II injection mechanism—i.e., electron injection directly from the ground state of the dye into the semiconductor conduction band without the involvement of excited dye molecular states. In contrast, the so-called type I injection involves electron transfer from an excited state of the dye (e.g., the LUMO or LUMO + 1 orbitals localized on the dye close to the interface) populated upon photoexcitation.

To investigate the possibility of direct transitions, a TDDFT calculation was performed on the $[Ti_{17}O_{24}(OH)_{16}(NPA)_4]$ model (Table S7, Supporting Information). Due to the large size of the system, only the first 10 excited states were obtained. The third and seventh excited states possess relatively large oscillator strengths of 0.1391 and 0.1059 au, repectively. The photoexcited electron population for both states is occupied in the LUMO + 2 and LUMO + 3 of the $[Ti_{17}O_{24}(OH)_{16}(NPA)_4]$ model. These virtual orbitals as well as the LUMO and LUMO + 1 are quasi-4-fold degenerate with an energy of 3.76 eV and correspond to the LUMO of the free NPA. Thus, nine of the 10 lowest energy transitions are effectively excitations into NPA orbitals that do not overlap with titanium. Only the ninth excited state, corresponding to an excitation wavelength of 357 nm and possessing a relatively small oscillator stength, shows population of the photoexcited electron on the $\mathbf{Ti_{17}}$ cluster, a direct consequence of populating the mixed Ti/NPA orbitals. Given the optical strength of the HOMO−LUMO + 1 transition in **NPA-H**, other strong direct sensitizer-to-Ti transitions undoubtedly occur beyond the first 10 excited states calculated here.

To the best of our knowledge, this is the first example of an IET simulation involving multiple independent sensitizers in close proximity, attached to a semiconductor surface that is fully structurally characterized by X-ray diffraction. Given the high loading densities, typically observed in DSSCs, it is highly probable that surfaces with chromophores in close proximity exist in these devices. While chromophores are generally considered electronically isolated with respect to neighboring sensitizers, our calculations show that this is not necessarily the case. For the LUMO + 2 transition, the excited electron diffuses through the Ti/O core and relocalizes on an NPA molecule on the opposite side of the cluster; density from a single excitation is observed on two sensitizer molecules simultaneously. Delocalization of electron density from an excited sensitizer onto neighboring sensitizer molecules could reduce the ability of the neighboring molecules to absorb light effectively, thereby reducing the efficiency of the device. Furthermore, delocalization of an excitation over multiple chromophores may lead to increased rates of charge transfer to redox shuttles that would also detrimentally impact device performance.

The strong mixing of the LUMO + 1 state with the cluster orbitals also has important implications for light-harvesting systems. An increase in the broadening of a sensitizer injecting state, upon coupling to the substrate, is associated with increased rates of electron transfer.[39] Similar behavior is observed in the calculated IET rates for $[Ti_{17}O_{24}(OH)_{16}(NPA)_4]$. While the **NPA** LUMO + 2 and LUMO + 3 states do not split or shift upon complexation to the POT cluster (no broadening), the LUMO + 1 state does contribute to several new states and is effectively broadened over an energy range of approximately 1 eV. Initial rates of IET from the LUMO + 2 and LUMO + 3 states are similar at 0.02 and 0.03 fs^{-1}, respectively, and are considerably less rapid than the rate of injection from the LUMO + 1 state, which is nearly an order of magnitude faster at 0.19 fs^{-1}.

Given the fast injection and the low energy of the transition relative to the LUMO + 2 and LUMO + 3 states, injection from the **NPA** LUMO + 1 appears to be ideal. In addition, direct injection through a type II mechanism should be possible. However, the formation of new energetically isolated orbitals below the quasiconduction band could mean that direct excitation into these orbitals might not lead to injection into the semiconductor substrate. Instead, the excitation may remain localized on these orbitals and such states may even act as low energy sinks for higher-energy excitations.

■ CONCLUSIONS

As part of our project on single-crystal analyses of functionalized Ti/O nanoclusters,[17,19] the structure of the polyoxotitanate nanocluster $Ti_{17}O_{24}(OPr^i)_{20}$ functionalized with four *p*-nitrophenyl acetylacetone (**NPA-H**) adsorbates has been resolved by single crystal X-ray diffraction methods, revealing the exact way in which the acac anchor group attaches to the semiconductor surface via bidentate chelation, as previously predicted by computational modeling.[10] The crystalline nature of the nanoclusters has allowed us, for the first time, to perform both spectroscopy and simulations for the same model structures of photosensitizer dyes on semiconductor surfaces. We find evidence of photoinduced IET, even at $\lambda > 400$ nm, as revealed by EPR spectroscopy and the analysis of the electronic structure at the DFT level. Theoretical calculations based on the functionalized cluster are used to predict the electronic properties relevant to light-harvesting devices. The density of states plot reveals that many of the unoccupied states of the free **NPA-H** are unaffected upon binding to the $\mathbf{Ti_{17}}$ cluster; however, the **NPA-H** LUMO + 1 states mix with cluster orbitals near the quasiconduction band edge, resulting in new states that are lower in energy by approximately 0.5 eV and have both **NPA** and Ti character. This mixing is expected to facilitate direct IET and a significant increase in the rate of IET.

Delocalization of the excitation over multiple chromophores is also identified.

■ ASSOCIATED CONTENT

Supporting Information

Additional figures of $Ti_{17}NPA_4$ complex and IET simulations, tables of crystallographic information, CSD refcodes for titanium acetylacetone structures, TD-DFT results, the full ref 31, and .cif file for $Ti_{17}NPA_4 \cdot 7C_6H_6$. This material is available free of charge via the Internet at http://pubs.acs.org.

■ AUTHOR INFORMATION

Corresponding Author

jbb6@buffalo.edu; robert.crabtree@yale.edu; gary.brudvig@yale.edu; coppens@buffalo.edu; victor.batista@yale.edu

Notes

The authors declare no competing financial interest.

■ ACKNOWLEDGMENTS

The authors acknowledge support from the Chemical Sciences, Geosciences, and Biosciences Division, Office of Basic Energy Sciences, Office of Science, U.S. DOE (Grants DE-FG02-07ER15909 and DE-FG02-02ER15372). The development of methods for simulations of quantum dynamics was supported by the NSF grant CHE 0911520, and the development of computational structural models of TiO_2 was supported by the grant CHE ECCS-0404191.

■ REFERENCES

(1) Gratzel, M. *Acc. Chem. Res.* **2009**, *42*, 1788.
(2) Hamann, T. W.; Jensen, R. A.; Martinson, A. B. F.; Ryswyk, H. V.; Hupp, J. T. *Energy Environ. Sci* **2008**, *1*, 66.
(3) Mishra, A.; Fischer, M. K. R.; Baeuerle, P. *Angew. Chem., Int. Ed.* **2009**, *48*, 2474.
(4) Lee, J.-K.; Yang, M. *Mater. Sci. Eng., B* **2011**, *176*, 1142.
(5) Duncan, W. R.; Prezhdo, O. V. *Annu. Rev. Phys. Chem.* **2007**, *58*, 143.
(6) Persson, P.; Ojamae, L. *Chem. Phys. Lett.* **2000**, *321*, 302.
(7) Persson, P.; Lundqvist, M. J. *J. Phys. Chem. B* **2005**, *109*, 11918.
(8) Li, G.; Sproviero, E. M.; McNamara, W. R.; Snoeberger, R. C., III; Crabtree, R. H.; Brudvig, G. W.; Batista, V. S. *J. Phys. Chem. B* **2010**, *114*, 14214.
(9) Rego, L. G. C.; Batista, V. S. *J. Am. Chem. Soc.* **2003**, *125*, 7989.
(10) McNamara, W. R.; Snoeberger, R. C.; Li, G. H.; Schleicher, J. M.; Cady, C. W.; Poyatos, M.; Schmuttenmaer, C. A.; Crabtree, R. H.; Brudvig, G. W.; Batista, V. S. *J. Am. Chem. Soc.* **2008**, *130*, 14329.
(11) Abuabara, S. G.; Rego, L. G. C.; Batista, V. S. *J. Am. Chem. Soc.* **2005**, *127*, 18234.
(12) Xiao, D. Q.; Martini, L. A.; Snoeberger, R. C.; Crabtree, R. H.; Batista, V. S. *J. Am. Chem. Soc.* **2011**, *133*, 9014.
(13) Anfuso, C. L.; Snoeberger, R. C.; Ricks, A. M.; Liu, W. M.; Xiao, D. Q.; Batista, V. S.; Lian, T. Q. *J. Am. Chem. Soc.* **2011**, *133*, 6922.
(14) McNamara, W. R.; Milot, R. L.; Song, H. E.; Snoeberger, R. C.; Batista, V. S.; Schmuttenmaer, C. A.; Brudvig, G. W.; Crabtree, R. H. *Energy Environ. Sci.* **2010**, *3*, 917.
(15) Jin, S. Y.; Snoeberger, R. C.; Issac, A.; Stockwell, D.; Batista, V. S.; Lian, T. Q. *J. Phys. Chem. B* **2010**, *114*, 14309.
(16) McNamara, W. R.; Snoeberger, R. C.; Li, G. H.; Richter, C.; Allen, L. J.; Milot, R. L.; Schmuttenmaer, C. A.; Crabtree, R. H.; Brudvig, G. W.; Batista, V. S. *Energy Environ. Sci.* **2009**, *2*, 1173.
(17) Benedict, J. B.; Coppens, P. *J. Am. Chem. Soc.* **2010**, *132*, 2938.
(18) Li, G.; Dimitrijevic, N. M.; Chen, L.; Nichols, J. M.; Rajh, T.; Gray, K. A. *J. Am. Chem. Soc.* **2008**, *130*, 5402.
(19) Benedict, J. B.; Freindorf, R.; Trzop, E.; Cogswell, J.; Coppens, P. *J. Am. Chem. Soc.* **2010**, *132*, 13669.
(20) Cochet, S.; Rozes, L.; Popall, M.; Sanchez, C. *Mater. Sci. Eng., C* **2007**, *27*, 1401.
(21) Rozes, L.; Sanchez, C. *Chem. Soc. Rev.* **2011**, *40*, 1006.
(22) Steunou, N.; Kickelbick, G.; Boubekeur, K.; Sanchez, C. *J. Chem. Soc., Dalton Trans.* **1999**, 3653.
(23) Jiang, Y. W.; Wu, N.; Wu, H. H.; He, M. Y. *Synlett* **2005**, 2731.
(24) *Jaguar 7*; Schrodinger, LLC, New York, 2010.
(25) Dreuw, A.; Fleming, G. R.; Head-Gordon, M. *J. Phys. Chem. B* **2003**, *107*, 6500.
(26) Tozer, D. J.; Amos, R. D.; Handy, N. C.; Roos, B. O.; Serrano-Andres, L. *Mol. Phys.* **1999**, *97*, 859.
(27) Sobolewski, A. L.; Domcke, W. *Chem. Phys.* **2003**, *294*, 73.
(28) Dreuw, A.; Fleming, G. R.; Head-Gordon, M. *Phys. Chem. Chem. Phys.* **2003**, *5*, 3247.
(29) Tozer, D. J.; Handy, N. C. *J. Chem. Phys.* **1998**, *109*, 10180.
(30) Dreuw, A.; Head-Gordon, M. *J. Am. Chem. Soc.* **2004**, *126*, 4007.
(31) Frisch, M. J.; et al. *Gaussian 09*; Gaussian, Wallingford, CT, 2009.
(32) Allen, F. H. *Acta Crystallogr. B* **2002**, *58*, 380.
(33) Hurum, D. C.; Agrios, A. G.; Gray, K. A.; Rajh, T.; Thurnauer, M. C. *J. Phys. Chem. B* **2003**, *107*, 4545.
(34) Kerssen, J.; Volger, J. *Physica* **1973**, *69*, 535.
(35) Meriaudeau, P.; Che, M.; Jorgensen, C. K. *Chem. Phys. Lett.* **1970**, *5*, 131.
(36) Dimitrijevic, N. M.; Poluektov, O. G.; Saponjic, Z. V.; Rajh, T. *J. Phys. Chem. B* **2006**, *110*, 25392.
(37) Dimitrijevic, N. M.; Saponjic, Z. V.; Rabatic, B. M.; Poluektov, O. G.; Rajh, T. *J. Phys. Chem. C.* **2007**, *111*, 14597.
(38) Rego, L. G. C.; Abuabara, S. G.; Batista, V. S. *J. Chem. Phys.* **2005**, 122.
(39) Persson, P.; Lundqvist, M. J.; Ernstorfer, R.; Goddard, W. A.; Willig, F. *J. Chem. Theory Comput.* **2006**, *2*, 441.